Embedded fibre optic sensors within additive layer manufactured components

Maier, Robert Raimund; MacPherson, William Neil; Barton, James; Carne, Mark; Swan, Mark; Sharma, John N.; Futter, Simon K.; Knox, David A; Jones, Benjamin J.S.; McCulloch, Scott

Published in:
IEEE Sensors Journal

DOI:
10.1109/JSEN.2012.2226574

Publication date:
2013

Embedded Fibre Optic Sensors within Additive Layer Manufactured Components

Robert R.J. Maier, William N. MacPherson, James S. Barton, Mark Carne, Mark Swan, John N. Sharma, Simon K. Futter, David A. Knox, Benjamin J.S. Jones and Scott McCulloch

***Abstract*— Smart materials with integrated sensing capabilities are now ubiquitous in many structures and devices manufactured from composite materials and they offer enhanced safety, reliability and efficiency in such smart devices.**

This paper explores the application of embedded sensors to components manufactured using Additive Layer Manufacturing (ALM) technology. ALM offers the ability to create physical parts with little or no restriction in shape and complexity. In this paper, optical fibre sensors incorporating fibre Bragg gratings (FBGs) were embedded inside a component made by, and during a powder-bed based, layer-by-layer, additive manufacturing process. A commercial EOS P730 system was used, where a laser is employed to sinter the polymeric powder into a three dimensional component.

The fibre embedding approach is based upon insertion of a 'fibre-carrier' component which replaces a removable 'place-holder' component during an interruption of the ALM build process.

Tensile test specimens fabricated this way have been subjected to extended cyclic tensile loading trials at low strain levels of up to 580 με. The test specimens demonstrated stable and reproducible responses over a period in excess of 720 days and 311,000 load cycles.

Polyimide (PI) and acrylic (PMMA) jacketed fibres have been trialled and the resulting deformations of the component through internal stresses depending on the fibre jacket type are discussed.

***Index Terms*— Additive Layer Manufacturing, embedded sensing, Fibre Bragg gratings, fibre optic sensing, rapid prototyping, rapid manufacturing, selective laser sintering / melting, strain sensing, temperature sensing.**

I. Introduction

Composite materials have revolutionised product design and engineering in many areas. In part, this revolution has been enabled by embedded sensors, which have resulted in improved reliability and functionality of such materials and components. The ability to continuously monitor conditions and parameters from within a structure has enabled and significantly extended the use of smart materials across many industries, where the sensing ability helps to ensure safe and reliable operation. In many cases, the technology has permitted a dramatic extension of safe operating conditions, thereby improving efficiencies, reducing costs and minimising downtimes due to faults. Optical fibre sensors have been at the forefront of this embedded sensing revolution.

Additive **L**ayer **M**anufacturing (ALM) has, over the past 3-5 years, rapidly grown from its use in the early days as a Rapid Prototyping tool, primarily used in visualisation, assembly and modelling, towards a highly flexible **R**apid **M**anufacturing (RM) tool capable of producing usable engineering components. RM offers the ability to create physical parts with little or no restriction in external, internal shape or complexity. This technology is now en route towards becoming the next revolution in manufacturing technology [1,2].

Although there are several different concepts of ALM technology, they all share a common approach in that components are constructed in a layer by layer build-up process. Material is added from a reservoir in the form of a powder, wire or liquid and solidified using thermal or photochemical processes, creating a 3-dimensional (3D) component of arbitrary shape and structure. Since the process is the reverse of conventional 'material removal' manufacturing, i.e. instead of working from the outside to the inside, the technology works from the inside to the outside, it is therefore easy to *gain* access to the centre of a component, and create complex internal structures and voids. Unique to this approach is the ability to manipulate the material properties during fabrication by varying the ratio of two or more base materials prior to solidification. Thus it is possible to produce components in which the material characteristics vary in a controllable manner throughout.

RM, based on ALM, is gaining an ever expanding foothold in the area of high value, low volume and custom tailored component production. The ability to change a design, scale its dimensions or apply other customisations without changes in tooling, has profound implications in bespoke high value component manufacturing.

In recent years, highly significant but much more subtle benefits of RM technology are being realised and combined with advances in materials technology. These additional benefits have the potential to cause a paradigm shift in engineering design and manufacture. For example, RM allows

Manuscript received May 20th 2012.

R.R.J. Maier, W.N. MacPherson and J.S. Barton are with the Institute of Photonics and Quantum Sciences, at Heriot-Watt University, Edinburgh EH14 4AS, UK. (Corresponding author e-mail: r.r.j.maier@hw.ac.uk).

M. Carne, M. Swan, J.N. Sharma, S.K. Futter, D.A. Knox, B.J.S. Jones and S. McCulloch are with AWE, Aldermaston, Reading, RG7 4PR, UK

An earlier version of this paper was presented at the 2011 IEEE Sensors Conference, Limerick, Ireland and was published in its proceedings

the manufacture of intricate internal designs which could not be manufactured using the conventional material removal manufacturing technology, such as sub-surface cooling channels located a fraction of a millimetre below a contoured surface, or the ability to create internal light weight network structures.

Component fabrication by RM enables previously unattainable design features and tailoring of material properties, such as gradual changes in stiffness across a component by modification of internal structures or material composition. Such design features are gradually being introduced and supported by design and modelling tools. Figure 1 shows a 'cut-open' cross section of a typical example of an advanced design, demonstrating the capability of current ALM technology. This component is a section of a light weight aircraft part manufactured from stainless steel by EADS. Many more examples exist [3] where the unique abilities of ALM are used to create parts with geometries and properties, which were hitherto impossible to manufacture by conventional methods.

Figure 1. **Left:** Lightweight aircraft component with internal mesh structure, made from stainless steel by EADS©. **Right:** A complex multifunctional engine block mount with integrated pipe work in stainless steel by Within Labs© [3].

RM structures can be highly complex and intricate and therefore require careful characterisation and testing to verify properties and performance are as expected. However, in marked contrast to conventional engineering components manufactured from bulk materials, the conditions of internal structures are not necessarily represented or transmitted to the outside of component where they could be easily detected by surface attached sensors. Internal structures can be damaged without a meaningful indication on the outer surface and only mechanical load testing, in some cases close to the strength limits of the component will reveal internal damages. The internal structure in the component, shown in Figure 1, is completely hidden from view in a completed component and the condition of the internal webbing struts are only visible by, for example, radiography which reveals breaks and major distortions, but gives no information about strain states and stress levels.

Although advances in computational power has dramatically improved the capabilities and finesse of modelling tools based on finite element (FE) analysis, and are ubiquitous on an engineers desk, modelling of even simple parts as shown in Figure 1, will push these tools to their limits due to the number of nodes required for accurate modelling. The combination of the limits in the modelling tools and the limitations of mechanical testing make it imperative to have a monitoring tool which is capable of measuring conditions from within a component.

Such a sensor technology will foster the acceptance of such new technologies into the engineering community and will provide experimental validation data for modeling tools.

Optical fibre sensors (OFS), in particular those based on FBG technology and distributed sensing [4,5], are seen as a potential solution to allow stress, strain and temperature monitoring from within a complex 3D component. The layer by layer build up process of ALM technologies makes it possible to install a sensor component as part of the RM process, thereby allowing interior structural monitoring in regions not normally accessible by any other means. The embedding of fibre Bragg gratings has been amply and successfully demonstrated in composite materials. However even in these now widely used application areas, fibre Bragg gratings can experience complex phenomena such as spectral distortions by point like transverse loading, micro bending, induced birefringence and spectral chirping leading to a widening of the spectral signature [6]. Previous work on embedding optical fibre sensors during RM used 'shape deposition' [7], 'fusion deposition' [8] and 'stereo-lithography' [9].

II. Powder- Bed based Additive Layer Manufacturing Technology

Perhaps one of the most widely used commercially available RM technology is based upon selective laser sintering of layer-by-layer build-up of 3D components in a bulk powder-bed. The materials which can be used in these systems range from polymers, mostly polyamide (PA) based, to a large variety of metals and metal alloys, including aluminium, stainless steel and titanium [10]. This technology, in the form of the EOS P730 system [EOS GmbH, Germany] was used to fabricate test components using pure and glass-filled 'Polyamide 12' materials, PA 2200 and PA 3200 GF respectively [11].

In the 'EOS' process 100-150 μm thick layers of powder (120 μm used here) with a typical particle size of 60 μm, were deposited on top of each other, and each layer was selectively sintered layer-by-layer, by scanning a focused laser across the surface (10.6 μm CO_2 laser, 35 – 40 W, spot size 350 μm, scan speed 3 to 4.5 m s^{-1}). The laser heated the material to just above its melting point, thereby allowing the loose powder to sinter together. The laser parameters given are only approximate values for guidance, since the detailed process parameters are highly complex and dynamically change throughout the build process.

Although many of the operating principles are common to RM processes irrespective of materials used, one notable difference in RM of polymeric materials compared to for example metals, is that the process takes place with the powder

material being heated to a temperature just below its melting point. This is to eliminate problems associated with the very large coefficients of thermal expansion (CTE) of the polymeric materials. If the process were to take place at room temperature then the localised heating as a result of the laser power would cause a large localised material displacement. This would induce significant distortions and result in problems in the powder bed, and the resultant component geometry. The build process therefore takes place at an elevated ambient temperature of 176°C, with the laser raising the local temperate by only a further 10°C to just above the melting point for the PA material used.

In contrast, the same process using metal powders takes place at, or just above, ambient temperature (25 to 45°C), however the process uses lasers of significantly higher power to achieve sintering.

The additive layer build-up technique employed in these systems, combined with the machine configuration, limits the installation of optical fibre sensors (OFS) to in-plane orientations only, but the component itself can be positioned in any orientation within the build volume, allowing a OFS to be placed in an arbitrary plane within the component. Care however, has to be taken with the slight anisotropy in mechanical properties relative to the build plane orientation [12].

The concept of in–bulk measurements was demonstrated here using ISO 3167:2003 tensile test specimens with a sensor fibre installed during the fabrication process. Several sensor positions were considered, but here we report the case of a sensor running parallel to the test specimen face (configuration #1) and also running at an angle with respect to the specimen faces (configuration #2).

In configuration #1, illustrated in Figure 2, the optical fibre sensor is installed in a plane 1 mm above the neutral axis, parallel to the principal surfaces. The sensor location was offset from the neutral axis, which makes it deliberately sensitive to bending.

In configuration #2, illustrated in Figure 3 the optical fibre sensor was installed in a 'tilted' plane, relative to the principal surfaces of the tensile test specimen. As stated earlier, a sensor can only be installed in the plane of the RM build process; therefore this component had to be built in a tilted orientation in the powder bed. This configuration was deliberately chosen to allow the investigation of in-plane shear stresses, to reveal potential weaknesses induced by the installation of the sensor fibre.

Strain sensing was carried out using FBGs written into 125 µm diameter standard single mode fibres (SMF-28 equivalent), by a phase mask technique, with resulting reflection spectra in the 1550 nm wavelength region. The FBGs used here were approximately 7 mm long resulting in a -3 dB spectral bandwidth of ~250 pm, and were located at the centre of the long axis of the tensile test specimen (TTS). In configuration #1, the optical fibre sensors were positioned 1 mm away from the neutral plane to allow bend testing of the specimens, and in configuration #2 the sensors were positioned within 0.1 mm of the neutral axis of the TTS.

Fibres with polyimide (PI) and acrylic (PMMA) jackets, outer diameters 155 and 250 µm respectively, were used. PI was selected due to it being compatible with the temperatures used in the EOS process. PI has a Vicat, i.e. 'softening' temperature, of approximately 220°C, whereas the PMMA jacket material has a very low viscosity at the upper operating temperatures. Indeed PMMA will have started to decompose at these temperatures, primarily by loss of plasticisers, resulting in a brittle jacket after the embedding process; however a few experiments with PMMA fibres were carried out, and are described below.

A. Installation of optical sensor fibres

A conventional 3D build process was carried out until the system reached the plane at which an OFS was to be installed, and at this point, the build process was paused to allow the insertion of the fibre. The partially built component remained inside the fragile and easily distorted loose powder bed, as the

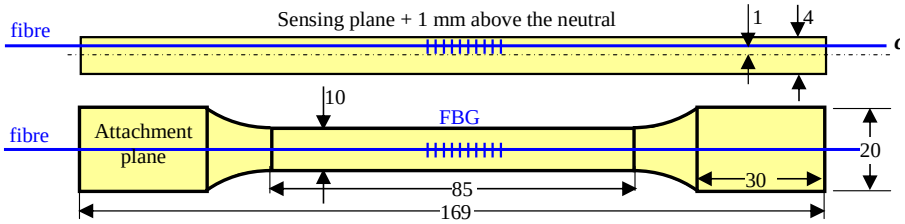

Figure 2. Schematic of an ISO 3167 tensile test specimen (TTS) with the location of the installed fibre for configuration #1 at a position of 1mm above the centre line "neutral axis" of the specimen. (all dimensions given in mm)

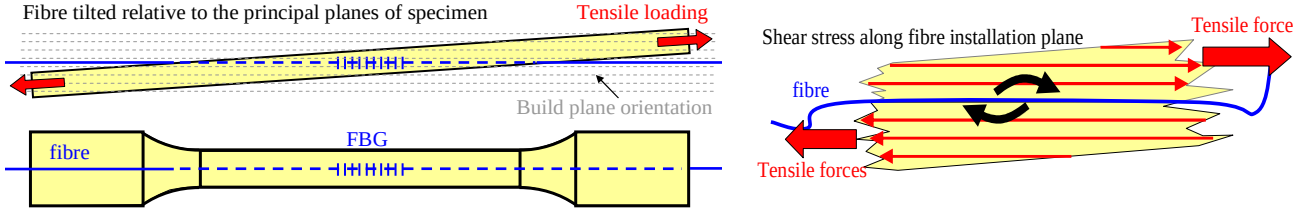

Figure 3. Configuration #2: The principal surfaces of the component and the plane of the installed sensor fibre are tilted relative to each other, to permit tensile testing of shear stress along the installed plane where the fibre is installed.

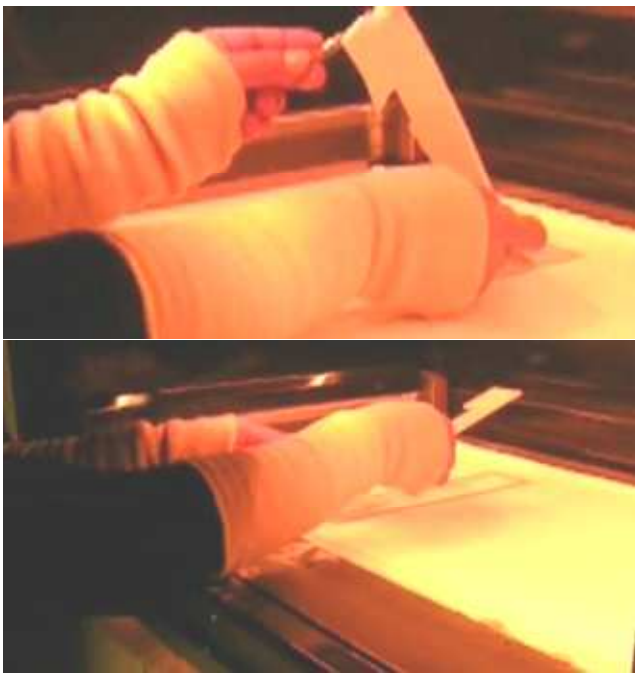

Figure 5. Top: Removal of hot and therefore 'soft' place holder from the power bed. Bottom: Insertion of pre built fibre holder with fibre into recess created by removal of place holder. This handling is currently done by hand but can be automated and improved by remote handling devices.

partially built part at this stage itself is not rigid, since at these temperatures the PA has not started to solidify. In order to insert the OFS, the build chamber was opened which caused significant cooling of the powder bed surface. It was therefore essential to be able to insert the fibre rapidly to minimise this effect. This process was not without its problems, however in a dedicated system such a process could be automated by use of robotics, which would not only be faster, but also permit handling at high temperatures.

The most critical issue with respect to the fibre sensor installation was to ensure that the fibre was in the correct location with respect to the partially built component, i.e. that it was straight, and was held in the plane of the powder bed. In order to ensure these parameters were adhered to, a location scheme was devised which consisted of a 'place-holder' component, which was built in parallel and partially surrounded the specimen in the powder bed.

This place-holder was carefully removed from the powder bed, providing a free space for the pre-built 'fibre-holder' component with the fibre sensor attached to it (see Figure 4). The fibre holder is important for a number of reasons: it keeps the fibre strained slightly to keep it straight, and so to avoid interference with the powder re-coater arm sweeping across the surface of the powder bed for subsequent powder deposition, following restart of the build process, it assists accurate placement of the fibre, and it simplifies the manual handling process. In order to enable splicing and termination of the fibre, an excess length of fibre was also required. Figure 5 illustrates the concept of the removal and replacement of the place-holder. Around the place-holder small sections of powder material were also sintered, to form a 'powder retention wall' which prevented loose powder in the powder bed from slipping into the void upon removal of the place-holder. The fibre-carrier was pre-manufactured in the same PA material, and its dimensions were calculated to allow for thermal expansion which will occur when the part is introduced into the chamber in its cold state however it is not essential that it is manufactured from the same material.

The removal of the place-holder was a delicate process, and although successfully carried out by hand, it would benefit significantly from an automated robotic process. Figure 4 shows two images from the actual place-holder removal (top) and insertion of the replacement fibre-carrier (bottom). In the top image, the soft state of the hot place-holder is clearly

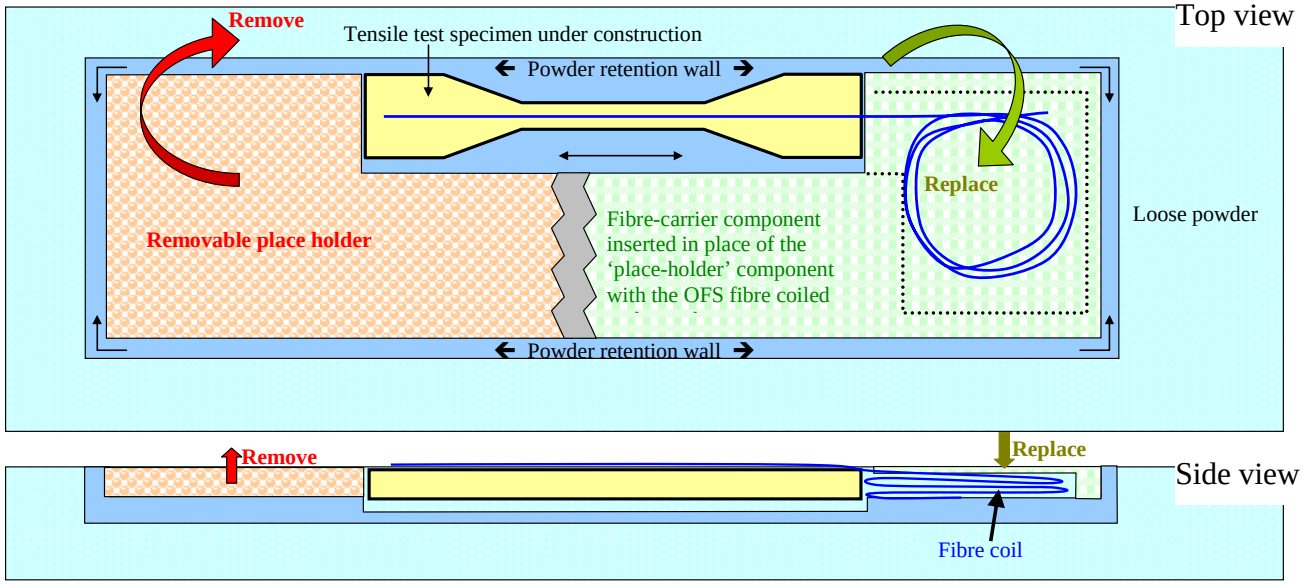

Figure 4. Schematic top and side view of the build area with the component under construction shown inside the powder-bed, surrounded by powder retaining walls. On the left, the removable place holder is shown, while on the right the replacement part with the fibre is shown which is inserted after removal of the place holder from the build volume.

visible by its pliant appearance.

Following the removal and replacement of the place-holder with the fibre-carrier, the build chamber was closed, and the system allowed to re-heat to its nominal operating temperature of 176°C. Since a typical optical fibre is slightly thicker than a normal build layer thickness, an extra thick layer of powder (typ. 220 µm) was applied, before the normal build process was resumed.

A test component with configuration #2 was specifically built to determine the mechanical stability of the component due to this additional thickness, and the presence of the optical fibre in the fabrication plane. The schematic arrangement of TTS, place-holder and other sub-components and structures inside the powder bed is shown in Figure 5.

A number of difficulties arise during manual handling of components inside the build chamber however they are expected to be absent during automated processing.

Due to the chamber being opened, thermal gradients occurred between the hot powder bed and the cooling build chamber, and so the specimens were observed to curl upwards resulting from contraction of the cooler top surface. Time was allowed for thermal equilibration between the surface of the powder bed and the partially built component, which allowed the part to settle down flat again before the build was continued, so not to abort the build process. Fibre curl has to be minimised as this would lead to the fibre location being disturbed when applying a new layer of powder on resuming the build process and this is achieved by a slight tensioning of the fibre on the fibre carrier inserted into the build process.

In addition, any slight pressure on the test bed, during replacement of the place-holder, could disturb the specimen. This affects the dimensional accuracy of the component being constructed.

At the end of the build process the system was allowed to cool down, and the finished component with the now embedded fibre sensor was removed from the powder bed in the normal manner for this build process. During this cooling down period, a compressive stress was generated within the OFS due to the large mismatch in CTE between the polymer and the fused silica fibre. This process was particularly pronounced for OFS with a PI jacket, although less so for PMMA jacketed ones. This is because PI is solid at the build temperature of 176°C, the shrinking PA (CTE= 110×10^{-6} K^{-1}) starts to impose a compressive force below its B50 Vicat temperature (~165°C), which eventually resulted in a compressive stress in the order of 2.1 GPa acting on the OFS at 20°C. This lead to a shift in the observed Bragg wavelength in the order of -32 nm compared to the pre-embedded Bragg wavelength. This is a large compressive strain of ~32000 µε acting on the OFS and under any other circumstances would result in a significant deflection (buckling) of the fibre. However, since the fibre is rigidly embedded in the polymer matrix, buckling will not occur, although the compressive stress can act to deform the component. Despite this very large compressive strain we do not observe degradation of the

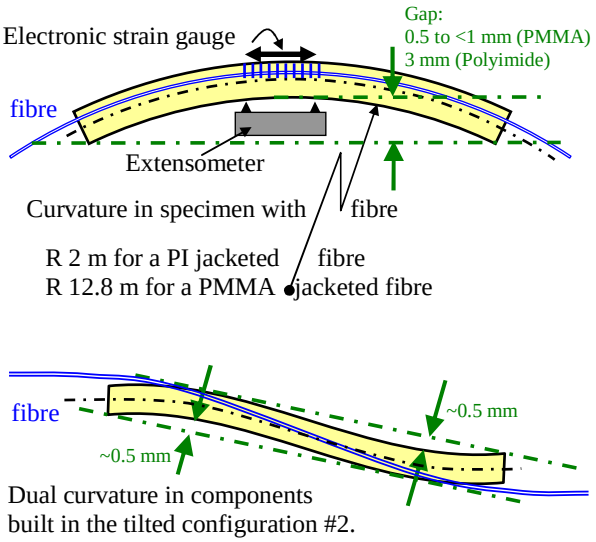

Figure 6. Top: Curvature in tensile test specimens (TTS) with embedded fibres and orientation of the curvature in relation to the position of the embedded fibre relative to the neutral plane. Bottom: The dual curvature in the 'tilted' configuration indicates that the curvature is due to the embedded fibre and not due to the interrupted build process.

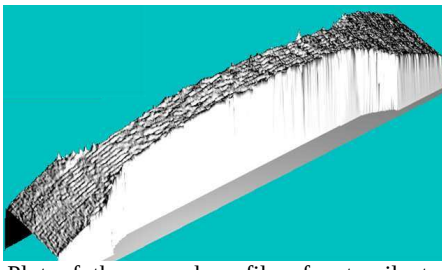

Figure 7. Plot of the curved profile of a tensile test specimen measured with a 3D coordinate measurement system. The elevation at the centre of the part is approximately 3mm and varies by ±0.5 mm from part to part.

spectral profile of the embedded FBG and the profiles look very similar to that shown in Figure 9 on the left.

In marked contrast, fibres with PMMA jackets only experience a compressive stress of ~0.5 GPa, generating a Bragg shift of -7 to -9 nm (three specimens) due to the marked lower Vicat temperature of PMMA (~103°C). This meant that only shrinkage of the PA below this temperature generated compressive forces.

The material properties of the PA material change dramatically over the build temperature range having a Young's modulus of near zero at the build temperature of 175°C to ~1.25 GPa at 25°C. The large compressive forces stored in the fibre located inside the PA components have an unfortunate effect of causing a distortion of the component, especially if the OFS was located off the neutral axis. The specimens exhibited curvatures of typically 0.47 m^{-1} and 0.078 m^{-1} (Figure 6 and Figure 7).

The curvature varies for components with different fibre jackets, as shown in Figure 6 (top) for specimens with PI, and PMMA fibre jackets respectively. Although this would indicate that PMMA fibre would be the preferred choice, since

they induce lower distortion, the compressive stresses cause micro bends, leading to strong distortions of the reflected Bragg grating spectra, and in addition, these specimens exhibited unpredictable and inconsistent strain transfer. This was due to the PMMA being very soft and unable to restrain and prevent the fibre from kinking during the early stages of the cooling down process.

PI jacketed fibres, despite the strong compression, were significantly more stable as will be shown in the experimental data.

During the initial stages of the experimental work it was argued that this deformation could also be due to the interruption of the build process. However, specimens manufactured subsequently, with a fibre installed at a tilt, were observed to exhibit dual and opposing curvature (see Figure 6 bottom). This suggests that the interruption of the build process is not the cause of the curvature and that the curvature is only due to the presence of the fibre in the specimen.

Although we report here the observation of curvature in the manufactured TTS, components which have the optical fibre sensor installed in the neutral plane will be significantly less affected by this effect. The thickness of the parts which have been manufactured for this project are accurate to ±0.1 mm (the thickness of each applied layer applied was 120 µm). The manufacturing accuracies enable the placement of the sensor fibre to within 150 µm of the neutral plane. The sensitivity to strain induced buckling and bending decreases strongly with overall thickness of the part and in components where the sensor fibre is embedded inside a thicker component, (typically 2 times the dimensions used here) the small offsets from the neutral plane will no longer be able to induce such curvature. The effect of fibre induced deformation has been magnified in these experiments by the selected geometry and embedding location. Despite this, it does indicate that care must be taken when instrumenting delicate (small dimension) polymer RM components. Parts manufactured in exactly the same process, including interruptions of the build process, but without inserted fibres do not exhibit any curvature or distortions and the component dimensional tolerances are <0.1 mm.

III. Tensile Strain Testing of Specimens With Integrated Sensors based on Fibre Bragg Gratings

We have carried out extensive tensile strain tests on the PA based tensile test specimens (TTS) which have been instrumented with PMMA and PI jacketed fibres containing BGs, but only PI fibres are reported here in detail since PMMA jacketed fibres performed poorly.

A dedicated strain rig has been designed for this long term test run where the tensile test specimen is held in between two highly flexible clamps to ensure pure tensile loading as shown in Figure 8. The actuation is carried out via a small pneumatic piston which moves approximately 15mm and which applies a force through a set of springs. The applied load is recorded in a load gauge at the top off the specimen and has been constant

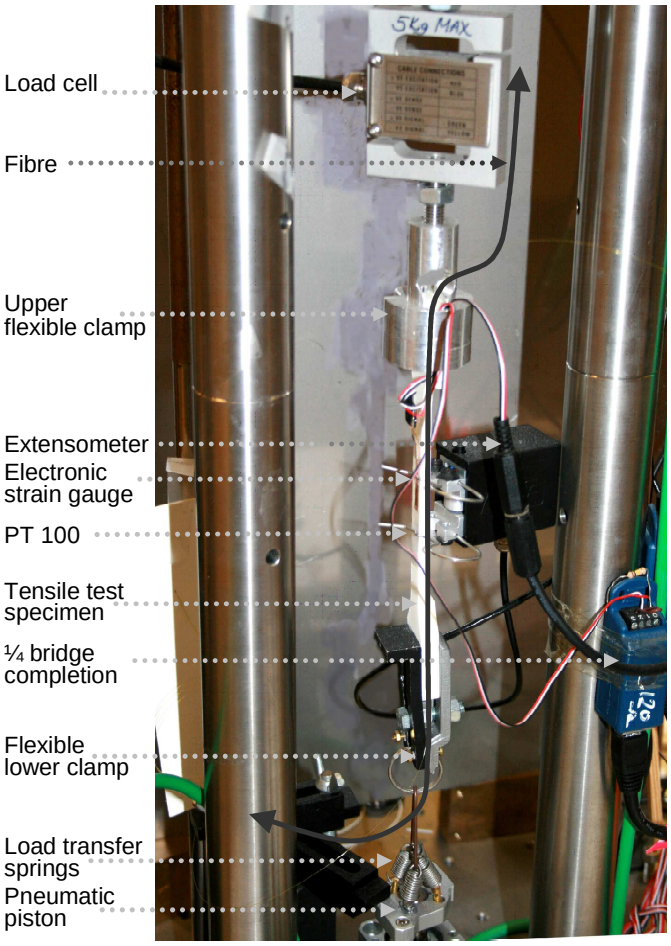

Figure 8. Tensile test sample mounted in free floating tensile test system showing from bottom up: pneumatic actuation piston, the spring loaded lower mounting, flexible lower mounting clamp, Nylon 12 tensile test specimen with extensometer attached to the right, electronic strain gauge between the clamps of the extensometer and the upper mounting point and the load cell at he very top. The arrangement only transfers longitudinal loads.

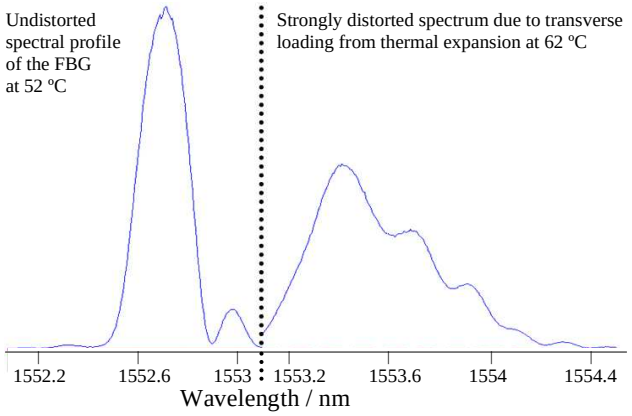

Figure 9. A typical example of the strong changes in spectral profile and grating strength observed during thermal cycling of FBGs embedded in glass filled nylon, indicating that this material combination is unsuited to the direct embedding of FBGs into the material during an RM process. The spectral shape on the left is representative of the spectra we observe for FBGs embedded in non glass filled Nylon, even at high compressive loadings leading to a -32 nm shift in Bragg wavelength.

throughout the experimental run with an accuracy of better than 5 %.

A. *Glass filled polyamide materials*

An experimental trial, not discussed here in detail, used glass filled PA (EOS PA 3200GF) as the specimen material. In the case of this material, bonding between the TTS and PI jacketed optical fibre was very inconsistent and the high glass fill fraction of ~30 % with an average glass bead size of typically 50 µm, induced transverse point loading on the FBG. Such point loading leads to a localised change in the refractive index through the stress optic coefficient. This in turn caused strong distortions in the Bragg grating spectrum. Figure 9 shows the strong changes to the spectral signature of an FBG embedded in a glass filled PA matrix. These changes varied between successive load cycles. In addition the overall sensor response to a cyclic strain exhibited strong hysteresis as shown in Figure 10. Together these properties make the combination of glass filled PA materials and embedded FBG unsuitable for sensing applications in the configuration used here.

A further indication of the somewhat weaker bonding between the TTS material and the embedded OFS, is the significantly reduced curvature of the finished part, due to the increased slippage in the presence of the glass beads.

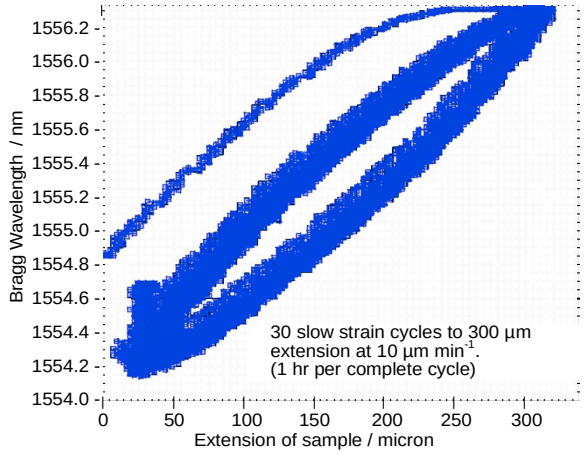

Figure 10. Cyclic loading experiment on a tensile test specimen manufactured from glass filled polyamide with an embedded fibre Bragg grating showing strong hysteresis.

B. *Embedded sensor in tilted build geometry*

The tilted experimental configuration, described earlier, was designed to elucidate possible interference between the installed sensor fibre and the mechanical and optical performance of the component. The critical issue here was the concern that the interruption of the build process, the addition of a somewhat thicker layer at the point of the embedded fibre, and the presence of the fibre itself would in someway modify the strength and response of the specimen to tensile loading. However, there has been no discernable difference between TTS built and configured in the tilted arrangement, i.e. where the build plane of a 'planar' finished TTS component was not aligned with the plane of the 3D build process. There were no measurable differences in mechanical strength of the finished component, and the integrated strain sensing capability of the embedded FBG was unaffected by the geometry of the build. However it has been shown that none of these issues were of concern.

C. *Planar build geometry (configuration #1)*

This is the main configuration tested and experimented on in this paper, where all principal planes are in parallel to each other.

Polymeric materials can have a somewhat complex time dependent stress-strain relationships but this complex behaviour is minimised at low speed tensile loading to small strains. The majority of characterisation measurements have been carried out at slow load rates or have been designed to use a small delay time between application of a load and the recording of a strain response to allow for the system to settle into a steady state following the load application.

The key experiment that has been carried out on a purpose built pneumatic driven load rig which has been continuously running for over two years (and is continuing at the time of writing this paper). Data from the embedded FBG were (and are) recorded once every 10 seconds by a Micron Optic sm125 interrogator, with an absolute accuracy of ±2 pm for the determination of the centroid of a FBG peak.

In addition to the embedded FBG, the specimen was equipped with a 120 Ω electrical strain gauge (6 mm long x 3 mm wide) attached to the outside of TTS in close proximity to the embedded fibre sensor. The strain data were read out by a National Instruments NI 9237 data acquisition device with a quarter bridge completion adaptor 9944. The strain gauge is not temperature compensated for Nylon but is a standard aluminium strain gauge. Scaling of the strain readings are carried out in Labview Signal Express and DAQmx through a built in calibration routine. Furthermore, a 25 mm gauge length extensometer is attached to the same central location of the TTS, as is a Pt 100 temperature sensor. All four data streams reporting strain, temperature and applied load, were time stamped and recorded using LabView™ software.

Tensile loading, cycling by ~25 N, between 8 and 33 N, was applied to a specimen for 100 seconds, over a period of 720 days. A loading change of 25 N caused a tensile extension in the centre of the specimen of 580 µε ($m \times m^{-1} \times 10^{-6}$) which is somewhat larger than a typical Young's modulus of 1.25 GPa, however, the elastic modulus of Nylon 12 samples manufactured by ALM are expected to be lower and in this case are in the order of 1.1 GPa. The transition time between the applied strains is in the order of three to four seconds.

Figure 11 shows the stable correlation of strain recorded using the electronic strain gauge versus FBG wavelength over the whole period of the experiment (720 days), indicating an embedded strain coefficient of 0.98 pm $\mu\varepsilon^{-1}$.

Data shown here have been temperature corrected by an externally applied Pt100 sensor to 20ºC as best as possible, however there remains a considerable common drift in all

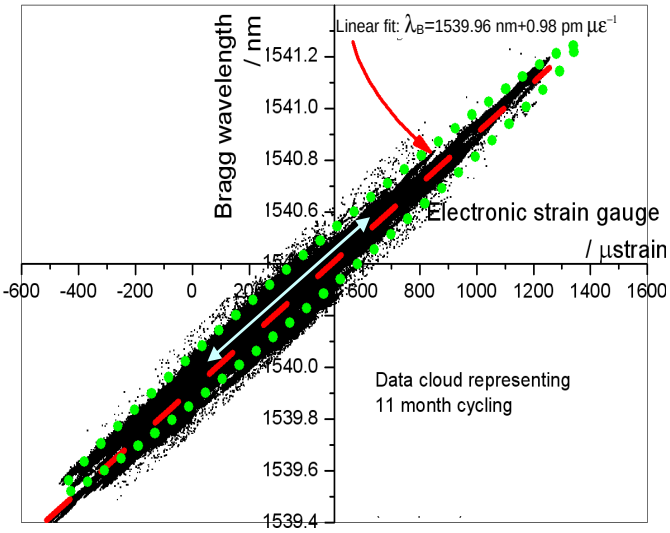

Figure 11. Correlation between strain and Bragg wavelength shift giving a strain coefficient of 0.98 pm με^{-1}. The data cloud here represents 11 months of nearly continuous cycling with 704,000 data points. The great majority of data points lie within the elliptical area marked by the dotted line. Some of the deviations observed are due to the synchronisation between the FBG and electronic strain measurements.

(Note: The double headed arrow at the centre of the cloud indicates the scale of a single strain cycle of approx 580 με, the overall extent of the data cloud in X and Y is not representative of a single strain cycle and includes temperature drift of the experimental system.)

three strain records (see also Figure 12) which has been attributed to an increase in the applied strain through an expansion of the test rig which is not corrected by the temperature sensor located on the tensile strain specimen. A temperature correction coefficient of 135 pm K^{-1} has been used for this correction. The CTE of Nylon 12 is 110×10^{-6} K^{-1} and the temperature coefficient of the FBGs used here are in the order of 10.95 pm K^{-1}. The correction coefficient has been determined experimentally by trial and error over the whole dataset and at 135 pm K^{-1} the majority of diurnal and seasonal variations of typically 3 to 4 ºC (day/ night) and 3 to 6 ºC (seasonal) were eliminated. However for optimum corrections of short term measurements a slightly lower temperature correction coefficient of 125 pm K^{-1} would be optimal. Since the key aim of this paper has been the investigation of the long term stability of the system over a period of 2 years it was decided to use the best correction for long term rather than short term.

A close-up of two and a half load cycles over ten minutes is shown in Figure 12 on the right, comparing the strain recorded using the embedded FBG (top), with an externally attached extensometer (bottom), and the reading from the electronic strain gauge (middle).

The FBG strain response truthfully follows the extensometer and strain gauge reading. Although the load is applied near instantaneous (within three seconds), the dynamic response showed a slight time lag and creep characteristic on loading and unloading, which is characteristic for polymeric materials, even at such low tensile loads and loading rates.

The main panel of Figure 12 (left), shows a cyclic loading trial of 311,000 load cycles lasting 720 days. During the first part of the experiment to day 150, we observed a gradual increase in applied strain which was visible in all three sensors on the test piece. This was due to a general increase in ambient temperature in the lab during summer, leading to a slightly higher applied load; this returned back to a lower temperature, and lower load, over the winter (day 148= 1stAug, day 270= 1stDec).

The difference in absolute strain recorded by the three sensing devices was due to their differing locations on the specimen and the curvature of the sample (Figure 6). During loading, the specimen was being straightened which lead to a slight compression on the convex side of the test specimen where the electronic strain gauge was attached, and also the FBG is embedded on the convex side of the neutral plane. Conversely, this straightening of the specimen during an applied load leads to an extension in the concave side of the specimen, where the extensometer is attached. Hence they recorded a lower and a higher strain value respectively. The deviations from the strain recorded in the FBG are of the correct magnitude to describe the change in shape during tensile loading. The data shown in Figure 11 and Figure 12 demonstrate a highly successful application of the fibre embedding technology during a RM process using PI jacketed fibres. The system response is stable and creep free within a few percent as shown in Figure 13, where the maximum deviation in readings between the three strain recording devices is <3 %. A significant fraction of this error is due to a gradual change in shape of the component, i.e. straightening, under the cyclic tensile load as is expected in polymeric materials after many thousands of load cycles, even under such low load conditions.

The stability of the strain record from the embedded PI jacketed OFS is remarkable, in view of the immense compressive pre-loading of the fibre. A parallel trial using a PMMA jacketed fibre is described below in section III D.

The majority of noise on the signal shown in Figure 13 can be explained by an incomplete temperature correction of the strain record data. Although a Pt 100 sensor is attached to the surface of the TTS, on the opposite side of the resistive strain gauge, in between the 'jaws' of the extensometer, there will be temperature gradients, and time lag between the temperature records of the Pt 100 sensor and the actual temperature at the sensor location. In particular the surface mounted resistive strain gauge will be more sensitive to transient short term changes in the lab temperature compared to the embedded FBG, which is buffered by the thermal mass of the polymer component, in which it is embedded. The large CTE of the polymer matrix (~110×10^{-6} K^{-1}) means that a minor temperate difference of 0.1°C between different measurement locations resulted in a 11 με difference of strain, or an error in temperature corrected strain which represents a difference of ~2.3 % of total strain applied.

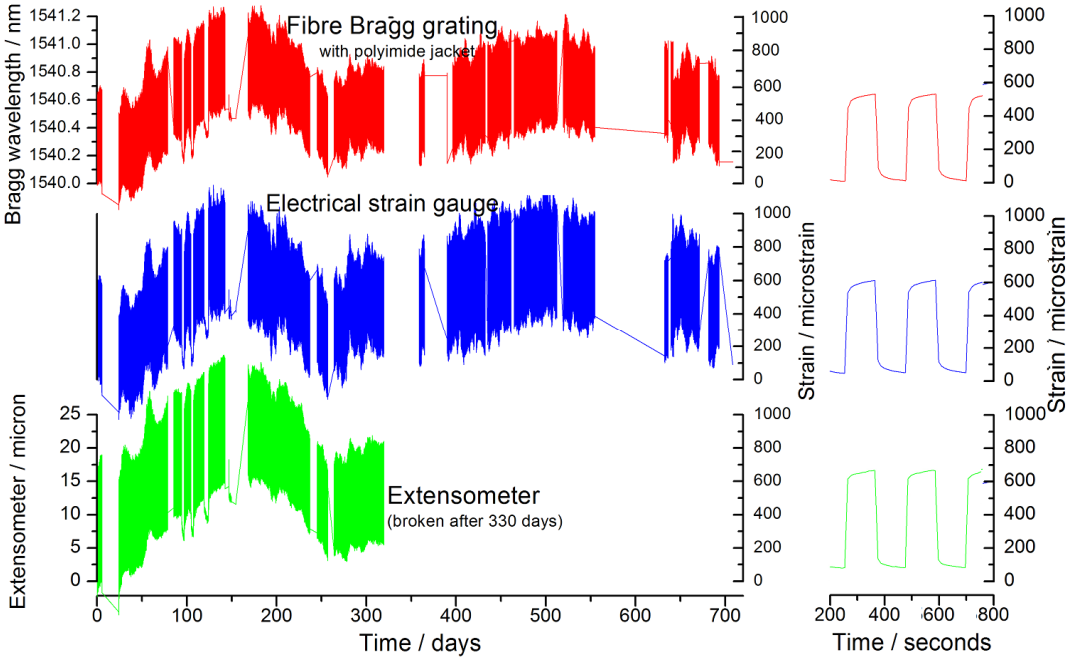

Figure 12. Left: 700 day load cycling experiment showing the stability of the sensor response. The overall drift in the applied strain is due to temperature changes over the summer periods (day 148=1st Aug). The top, middle and bottom traces show the response of the FBG, the electronic strain gauge and the extensometer respectively. The different scaling of the strain response is due to the change in curvature of the specimen on applying the tensile load. Right: The graph on the right shows a close up of 2 ½ load cycles over a period of 10 minutes at the start of the experiment showing (from top to bottom) the change in Bragg wavelength, the strain recorded by the electrical strain gauge and the reading from the extensometer.

D. PMMA jacketed fibres

In contrast, to the experiments described above, in a parallel trail using PMMA jacketed OFS embedded in a PA specimen, the embedded fibres exhibit a compressive Bragg shift of only -7 to -9 nm. However these trials were less successful primarily due to the reason that the fibre was deflected from straight under compressive load since the soft PMMA will not restrain the fibre sufficiently in its lateral position. This leads to micro-bending and distortions in the FBG spectrum. Tensile loads applied to a fibre with micro-bends will initially release the micro bends before creating a change in strain in the OFS which will modify the reflected Bragg wavelength from the FBG.

The equivalent trial to that shown in Figure 12 using a PMMA jacketed fibre over a period of 30 days, showed a continuous upwards creep of the strain recorded in the FBG of about 70-90 με per day. In addition to this creep behaviour, a strong distortion of the FBG spectrum, from a clean bell-shaped profile with ~280 pm bandwidth at -3dB before installation, to a highly structured spectrum over a bandwidth of 3 nm in the PMMA fibre, indicated uncontrolled and inhomogeneous bonding between the TTS and the optical fibre sensor (OFS), possibly coupled with micro bends. The spectral profile also was changing over time, indicating insufficient bonding and retention of the embedded OFS in the polymer matrix.

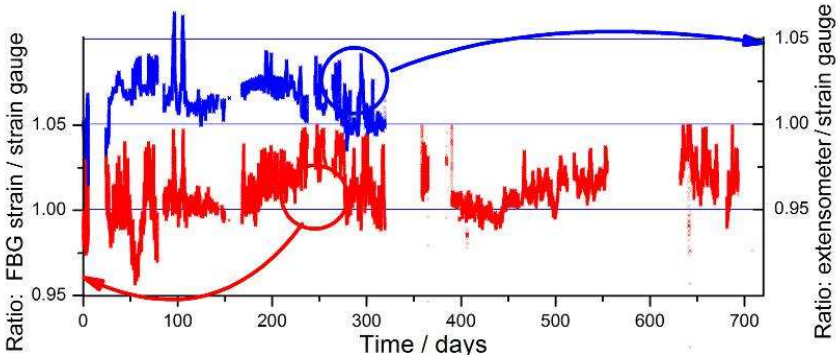

Figure 13 Ratio between strain measurements from the embedded fibre Bragg grating and the attached electrical (resistive) strain gauge (lower curve and left Y-scale) and the ratio of the strains recorded by the extensometer and the electrical strain gauge. Since FBG and strain gauge are on the same side, off the centre line (FBG: +1 mm; strain gauge: +2 mm), they should record an ideal ratio of 1. However since there is a small curvature in the specimen which is partially eliminated under tensile load, the readings will deviate from '1' by a small amount. Extensometer and strain gauge are on opposite sides of the centre line (see Figure 6) and a straightening will cause a shift of the ratio from '1' towards higher values.

IV. CONCLUSIONS

We have demonstrated successful sensor embedding in components manufactured by ALM technology with optical fibre sensors (OFS) based on fibre Bragg grating (FBG) strain sensors. Embedment of the fibre sensors has taken place as an integral part of the build cycle inside an EOS P730 ALM system.

The successfully embedded fibres have a PI jacket and the component material used in the successful embedding trial was Polyamide 12 (PA 2200).

In addition, fibres with PMMA jacket were trialled and glass filled PA was used as specimen material, and both were shown to be unsuitable for embedding due to weak and unstable strain transfer, and spectral changes in the FBG induced by point loading from the glass beads. PMMA jacketed fibres are furthermore unsuitable due to the high process temperature during RM which leads to a degradation of the PMMA jacket.

PI jacketed OFS are under very strong compressive load, after embedding, resulting in a Bragg wavelength shift of typically -32 nm. This high compression induces curvature in the specimen if the OFS is installed outside of a neutral bend plane.

The embedded OFS were tested over an extended period 720 days, at low cyclic strain levels of typically 580 με.

Data show that the embedded OFS system were stable over such extended time periods, and very high numbers of load cycles of which 311,000 are presented here, however the experiment is still ongoing and is now at cycle 350,000 without any changes to the response to those shown here.

It should be possible to transfer the procedure of embedding an OFS into other components during an ALM process, as demonstrated here in a polymeric material, to metallic material systems; provided the OFS to be embedded can be protected sufficiently from excessive thermal loading of the sintering laser. Early work by X.C. Li in 2000 to 2002 [10] has shown that, by using 1.5 mm thick electroplated nickel coatings, a fibre can be successfully embedded into stainless steel during a selective laser melting/sintering process, and that it is capable of being used as a sensor. However, the coating used in [10] is very thick, potentially interfering with the function of a component. Thinner coatings might be preferred which would lead to a significant increase in thermal loading on the OFS. In contrast to the high ambient processing temperatures in ALM of polymer systems (typ. 175°C), laser based ALM of metallic materials takes place at or around ambient temperature, and therefore some of the complexities of fibre insertion and handling presented in this paper are reduced.

Recent developments in high temperature compatible 'regenerated' FBG [13], raised our renewed interest in this field by potentially providing an embedded sensor configuration which not only is expected to survive a short term high temperature embedding process (typically 1430°C for stainless steel) with a potentially thinner protective metallic jacket compared to previous papers, but also provide sensing capabilities at high temperatures in the order of up to 1000°C. Such an embedded sensor technology would dramatically extend the operating regime of fibre optic strain sensors to previously unattainable temperatures.

REFERENCES

[1] Hopkinson N., Hague R.J.M. and Dickens P.M. *"Rapid Manufacturing: An Industrial Revolution For The Digital Age"*, John Wiley & Sons Ltd, ISBN 0470016132 (2006)

[2] Smith P., Rennie A., *"Development of an Additive Layer Manufacturing (ALM) selection tool for direct manufacture of products*". In: Solid Freeform Fabrication Symposium 2008. University of Texas at Austin,
ISBN 1053-2153 pp. 507-518. (2008)

[3] http://withinlab.com/case-studies/index7.php (May 2012)

[4] Maier R.R.J., MacPherson W.N., Barton J.S., McCulloch S., Jones B.J.S., *"Distributed sensing using Rayleigh scatter in polarization-maintaining fibres for transverse load sensing"*, Measurement Science & Technology, Vol.21, No.9, Art. No. 094019, SEP 2010

[5] Li Y., Liu W., Feng Y., Zhang H., *"Ultrasonic embedding of nickel-coated fibre Bragg grating in aluminium and associated sensing characteristics"*, Optical Fibre Technology, Vol.18, Issue 1, (2012)

[6] K.S.C. Kuang, R. Kenny, M.P. Whelan, W.J. Cantwell, P.R. Chalker, *"Embedded fibre Bragg grating sensors in advanced composite materials*", Composites Science and Technol., Vol.61, Issue 10, pp. 1379-1387 (2001)

[7] Li XC.; Prinz F., *"Embedded Fibre Bragg Grating Sensors in Polymer Structures Fabricated by Layered Manufacturing"*, J. of Material Processes, Vol.5, No.1, pp.78-86 (2003)

[8] Safari A., Danforth S.C., *"Development of novel piezo electric ceramics and composites for sensors and actuators by solid free-form fabrication"*, ISAF98, Int'l IEEE Symposium on Applications of Ferroelectrics, ISBN 0-7803-4959-8, pp 229-234 (1998)

[9] Nau W.H., *"Embedding sensors using stereo lithography"*, Master thesis, Clemenson University (1991)

[10] Li, X.C., Johnson J., Groza J., Prinz F., *"Processing and microstructures of fibre bragg grating sensors embedded in stainless steel"*, Metallurgical and Materials Transactions A; Vol.33, No.9, pp. 3019-3024 (2002)

[11] http://www.eos.info/pa-2200 and pa-3200-gf
accessed 15.5.2012

[12] Lee C.S., Kimb S.G., Kimb H.J., Ahnbet S.H., *"Measurement of anisotropic compressive strength of rapid prototyping parts"*, J. of Materials Processing Technology. Vol.187–188, pp.627–630 (2007)

[13] Bandyopadhyay S., Canning J., Biswas P., Stevenson M., and Dasgupta K., *"A study of regenerated gratings produced in germanosilicate fibres by high temperature annealing"*, Optics Express, Vol.19, Issue 2, pp. 1198-1206 (2011)